

Aaron D. Spooner  
Louisiana State University

26 July 2011

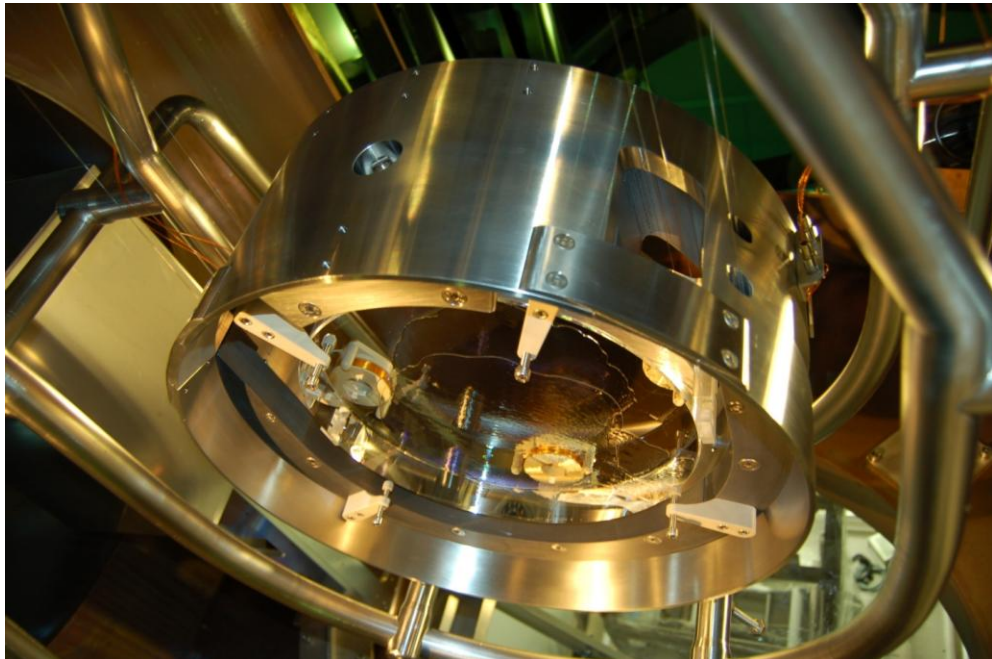
University of Florida International REU for Gravitational-Wave Physics

Host Institution: Sapienza  
Rome, Italy

Mentor: Paola Puppo

Project:

Understanding the properties of fused silica fibers for Virgo's current Gravitational Wave  
interferometer mirror suspensions



## Abstract

The purpose of this project is to understand the intrinsic properties of the fused silica fibers are installed in Virgo's current interferometric detector, Virgo experiment. These fibers will provide suspension for the Virgo interferometer mirrors. Significantly reducing thermal noise emissions, these fused silica fibers are highly implemented. Currently, the properties of the silica fiber are under further investigation. Utilizing various techniques to monitor the fiber's properties, investigational results will be analyzed and recorded prior to the fiber's installation. Additionally, realizing bonding methods for the fiber-mirror connection is another behavioral priority.

## 1 Introduction

### 1.1 Gravitational Waves

Introduced in 1916 and emerging from Einstein's general theory of relativity, gravitational waves are disturbances or perturbations in space-time. These propagations occur from accelerating non-symmetric mass distributors such as orbiting pulsars and black holes. However, these ripples in space-time are practically infinitesimal in length. Although indirectly verified as a result of discrepancies in pulsar 1916+13 predicted period, gravitational waves have not been detected as of date. Unlike, electromagnetic waves, gravitational waves propagate throughout the universe seamlessly. These waves do not interact with matter. From an experimental view point, such a detection may seem impossible or too improbable for accurate findings. On the contrary, several sites have been established to detect these perturbations in space-time. Using a Michelson-Morley Interferometer design, such sites known as LIGO, GEO600, and VIRGO have been constructed in order to accomplish this task. A shared concern for these detectors is the existence of external noises that inhibit instrument sensitivity and accurate detection. The subject of this report is based on a particular gravitational wave interferometer located in Cascina, Italy known as VIRGO. The Virgo interferometer houses a monolithic suspension design that encompasses a fused silica fiber as a means of reducing thermal noise activity.

### 1.2 Silica Fiber

As metallic wires produce thermal noise due to internal friction, the monolithic suspension design proved to be highly favorable. In more concrete detail, a low

dissipation material such as fused silica fibers are implemented in the Virgo gravitational wave detector as a more appropriate solution. In conjunction with the lack of thermal noise production, the material's breaking strength is highly trustworthy. In the early stages of the fiber's development, several designs were tested. The design of these fibers are constructed with extreme care and accuracy. Virgo in collaboration with McIntosh from the GEO600 group at Glasgow constructed the required machine for the production of such fibers. Mechanically and deliberately, the fiber is pulled from a previously synthetically fused silica rod. The fiber is heated from pure oxygen and hydrogen gas. Fibers constructed in this way have been "geometrically characterized" with a computerized microscope. However, this mechanical design for producing fibers has been modified in order to produce current fused silica fibers for testing. After producing the fused silica fiber, certain tests must be run in order to understand the behavior of the fiber. For instance, due to the sensitivity of the fiber's surface, any significant scratch can dramatically reduce the breaking strength of the fiber. In fact, the slightest contact with the fiber can break the fiber. These fibers must be handled with extreme care. This sensitivity was held in mind throughout the entire fused silica fiber installation process performed during this project. Another important aspect of these fibers' behavior is the events that lead up to a complete break in the material. Although having high degree of durability, it is important to understand the imperfections that accompany this system of suspension. In correlation to the fibers breaking point, understanding the effectiveness of the silica bond with current Virgo interferometer mirrors must also be taken into consideration.

## **2 Experimental Methods**

### **2.1 Experiment set up**

The apparatus and layout of the entire experiment has been confined to a vacuum chamber monitored via PC utilizing Vallen Acoustic Emission systems and programs. A specially designed mounting unit has been established to run preliminary tests on a 79.38 cm long Aluminum fiber. Attached above the mounting bracket and in direct contact with the given fiber, there rests an accelerometer with a denoted channel number. Likewise, another accelerometer with a different denoted channel number is attached to the top of a 5.6 kg test load. The designation of weight for the given test load was a direct result of proportionality to the interferometer's mirror weight in conjunction with its mounting system. The weight has been slightly adjusted to test the fiber at a greater strain. As testing practices improved and installation procedures mastered, the silica fiber was analyzed under this mounting mechanism. The purpose of this design is welcomed as it is required to simulate the expected "hang" length of the silica fiber as well as support its distinct vacuum chamber

design. The chamber design or "hat" has incorporated a metal with properties that appear to be closely related to most aluminum alloys as it is not magnetic. The mechanism stands at 1.1 m and has a base with a diameter of .60 m which supports the framework of the mechanism's mounting bracket. The circular base has inscribed within its surface a secondary ring that is required for O-ring insertion. This secondary ring is required for establishing a vacuum once the O-ring has been inserted. If the O-ring is not properly aligned with this inscribed ring then a proper vacuum cannot be achieved. After lowering the chamber, the apparatus is contained and the inside is only visible through a single viewing port .68 m above the ground. Fortunately, it is possible to see everything within the chamber. Unfortunately, a light source is required for better illumination and construction of this lighting system will be discussed at a later point in this report.



*Figure 1: mounting mechanism designed to support fiber (left) and the chamber (right) used to create a suitable vacuum to simulate Virgo conditions*

## 2.2 Early test with Aluminum fiber

To begin, understanding how to monitor the fused silica fiber was the main concern in the early stages of this project. Testing the sensitivity of the accelerometers and deriving a method of disturbance isolation served as the first challenge. In addition to the sensitivity of the accelerometer, initiating a direct,

even contact served as another task. Second, isolating the minute deformations within the wire proved to be extremely troublesome. Lastly, establishing a consistently stable platform as well as environment for the detectors provided an unwanted challenge that, nevertheless, had to be dealt with on a constant basis.

Initially using metallic clamps to keep the accelerometers in place, the surface contact of the accelerometers were appropriate and extra noise was nonexistent at that moment in time.

Realistically, the test load mounting design prevents the implementation of any externally attached mechanism such as a clamp. Additionally, the added weight would produce an unbalanced system for the test load. However, for that particular moment in time, the configuration was suitable for preliminary test runs. These tests allowed for further insight into the sensitivity of the accelerometer.

To pause for a moment, it is important to comprehend the mechanics of the accelerometers used in this experiment. An accelerometer measures the respective or proper acceleration. For the purpose of this experiment, piezoelectric accelerometers are implemented in order to study dynamic mechanical changes. Piezoelectric accelerometers are well known transducers for their remarkable ability to measure the exact vibrations of a given system. In this experiment, vibration within the given fiber can be detected with these piezoelectric instruments. An accelerometer also senses the surrounding seismic activity. Through electronic integration and computer interfacing, these piezoelectric devices can provide information pertaining to the velocity as well as displacement of any disturbance. With no external power supply or movable components, these instruments are incredibly compact and durable.

As spherical wave propagation registers at different moments in time between the two separately placed accelerometers, the detectors will record these distinct moments in time. With this statement in mind, the preliminary experiments consisted of hitting or tapping the test load in an effort to calculate the velocity of sound through the given metal. At this stage in the experiment, channel 2 was assigned to set a top the mounting bracket and channel 1 was placed on the test load hanging directly below. The Vallen Acquisition system was set to record as a metallic pressure vessel with the standard factory default settings. With the distance set at 13.5 centimeter which proved quite acceptable as it was chosen to be well within the diameter of the test load, vibrations were induced in five distinct, isolated hits. The hits or taps were oriented at certain corners of the surfaces in order to understand how the accelerometer would register the hits. As predicted, hits closer to the accelerometer appeared first with a greater amplitude and energy. In similar fashion, hits farther away produced shorter amplitudes and weaker energies. Using this information, the preset distance was divided by the difference in time of the two channels in order to produce the rate of propagation or speed. After reviewing the results, apparently the sensitivity of the Vallen Visual AE system is

insufficient. The problem emerges as the difference in time between channel 1 and channel 2 cannot be measured for values less than 100 micro seconds. Additionally, the zoom feature breaks down at a certain point and displays inaccurate scales. As the scale approaches set intervals of 100 micro seconds, the linear spacing of the chart fails to produce proportionality.

After understanding the vallen acquisition system, the next step involved establishing a suitable contact without the use of metallic clamps. As the provided magnetic clamping mechanism did not provide for a balanced system nor a suitable contact as a result of the material's weak magnetic attraction, wax was the appropriate and non invasive option. The applied wax must be uniformly distributed between the accelerometer and the surface on which it is being applied. Failure to establish a smooth, even contact results in extra noise in the Vallen Visual Acoustic Emission diagrams. Even though in most cases this noise was confined to a certain amplitude range, the interference inhibited proper analysis. In order to detect isolated incidences within and around the fiber, the system must maintain silence at all times. In reference to figure 2, the noise was confined to amplitudes ranging from 40 to 43.5 dB. This confinement allowed for proper background noise extraction. Knowing the set range of interference, it was possible to properly adjust the accelerometer. Eventually, with practice and small, evenly spaced coatings of wax, the system achieved an adequate silence level. As it was extremely difficult to eliminate all forms of background noise at this stage in testing, the elimination of interference induced by an uneven contact was a considerable achievement.

*Figure 2. Image of 5.6 kg test load with channel piezoelectric accelerometer attached and designated as channel 1 or "green" sensor*

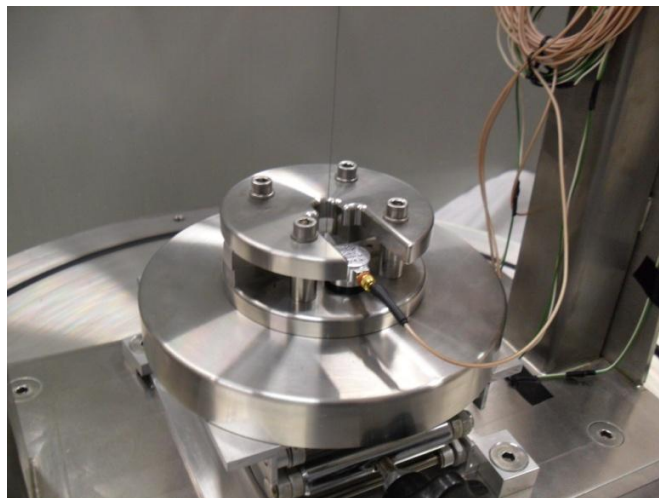
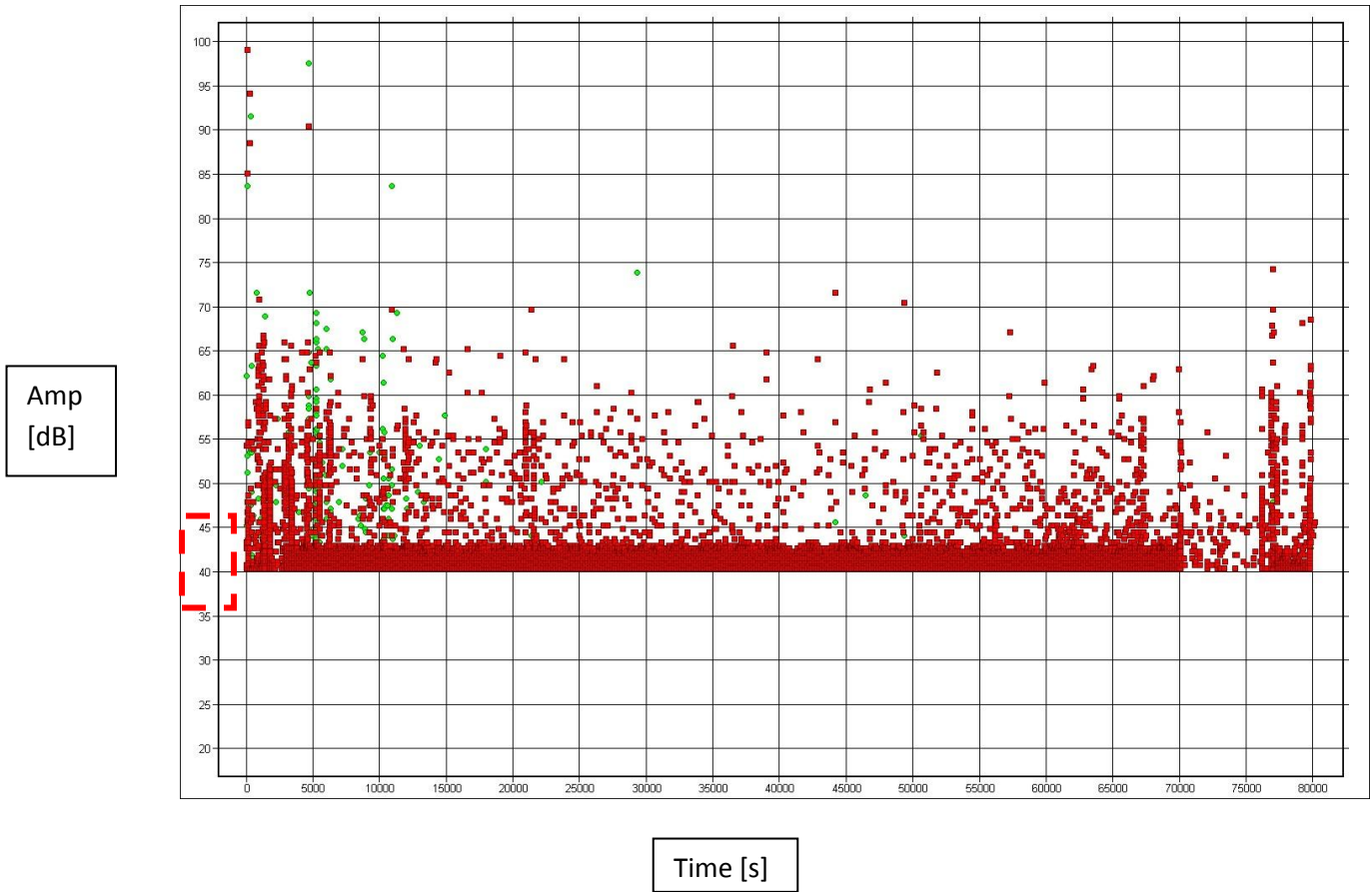


**Figure 3: Diagram illustrating improper wax distribution as indicated by an uneven surface or unbalanced accelerometer.**



### 2.3 Assembly of Vacuum Chamber

Preliminary tests were run on the Aluminum fiber with the Vallen Acoustic Emission system, assembly of the vacuum chamber began with locating and allocating special pipes. Next, while wearing latex gloves pipes must be thoroughly cleaned with alcohol before any connections are made. When every component has been properly cleaned, pipes are adjoined with O rings. After inserting these O rings into the rim of the pipe, clamps known as "ties" were attached around the adjoined pipes in order to establish an air tight system. Following pipe assembly, certain monitoring instruments were attached to open ended portions of the pipe. Specifically, the left port was designated as the air inlet and the right port functioned as a conduit to the Vacuum Gauge controller. The Vacuum Gauge provided digital readings of the pressure within the chamber. This device allowed one to determine whether or not the vacuum was sufficient for the purposes of the experiment.



**Figure 4:** Picture of pipe set up with air inlet (left) and Vacuum gauge sensor (right) attached.

Prior to configuration as an effort to optimize the vacuum and eliminate all leaks, the Leak Detector was implemented. This process incorporates  $^4\text{He}$  as a method of determining if there are any porous areas that could serve as potential air inlets. As a result of Helium's low mass and low percentage in atmosphere, this element is used in order to bombard a given area as a means of detecting a leak. Referred to as the "outside-inside" helium leak testing technique, the component being tested is connected to the detector and vacuum sealed. After establishing a vacuum within the attached component, Helium is sprayed over the entire surface. Within the detector, there lies a mass spectrometer.

If the Helium penetrates any portion of the component being tested then the mass spectrometer will detect the leaked Helium. As this system can detect leak rates up to  $1.8 \times 10^{-5}$  mbar, the detector was most favorable for the desired  $1 \times 10^{-4}$  vacuum.



**Figure 5:** Image of leak detector.

## 2.4 LED lighting system design for proper illumination

After assembling the vacuum chamber, it soon became apparent that the inside of the chamber was extremely dark. In response to this lack of visibility, a LED lighting system was designed in order to monitor the preliminary Aluminum fiber. The components of this system were quite simple. Using only a basic resistor, switch, 9 volt battery and LED; a light source was established and attached underneath the top mounting bracket.



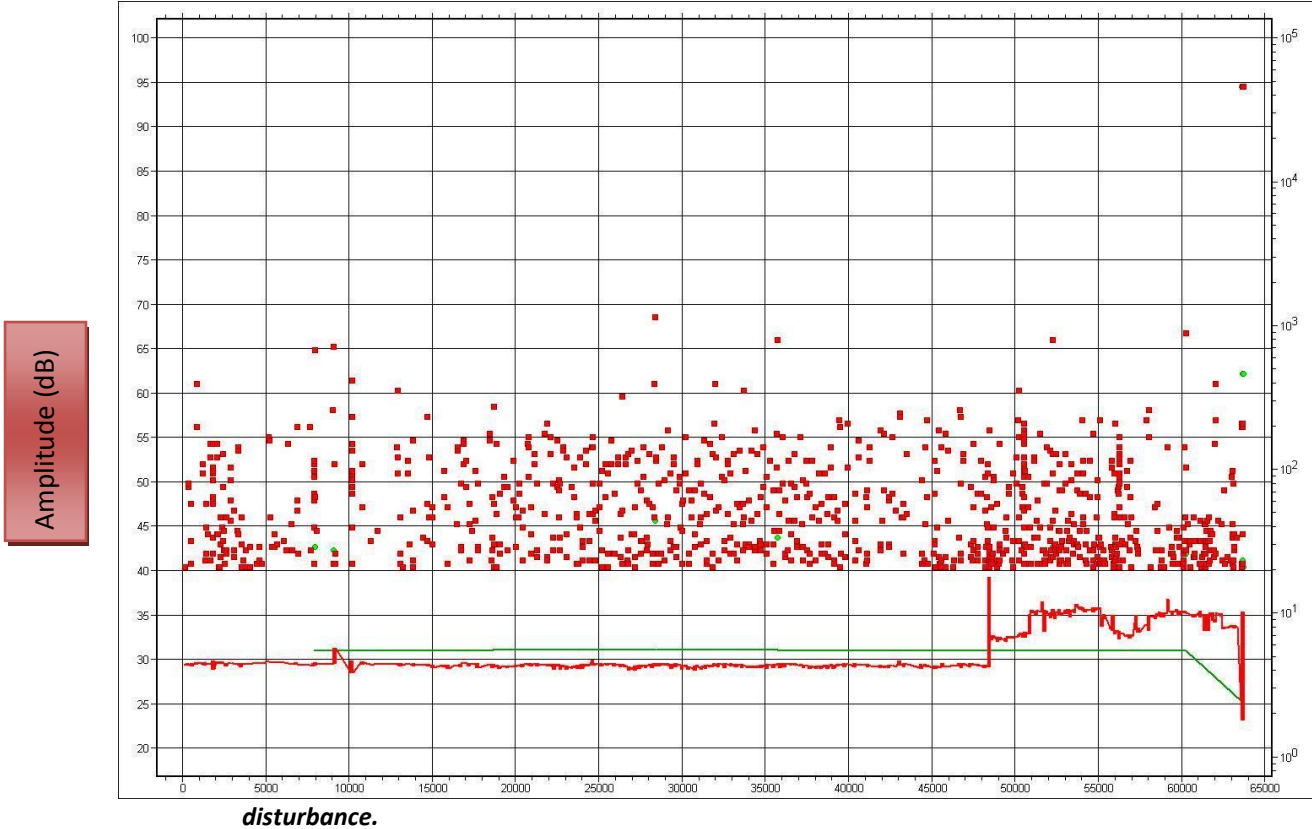
*Figure 6. LED lighting system control box*

## 2.5 Tests for the fused silica fiber

On July 4, 2011 installation day occurred. The fused silica wire was installed and setup tests were run in order to calibrate the accelerometers. With the surface under the attached accelerometer partially missing due to a gap within silica fiber's mounting ring, a poor contact was established. Despite the lack of surface area in contact, background noise did not appear as the accelerometer was properly aligned with a smooth, even wax coating. Several test were run after this installation. Also, at the end of most days, the Vallen Acoustic Emission system remained running throughout the night in order to detect any disturbances within or around the fiber. After compiling data for two weeks in this way, certain diagrams registered several disturbances. These disturbances were predicted to be micro crack detections. A micro crack can be defined as any

microscopic crack or fracture within the given material. Deformations could appear as slits or a rip with a wide assortment of geometries. Despite the impeccability of the material, these deformations could readily appear at any given moment in time as a result of a diminishing bonding strength in the material. Supporting the existence of micro cracks, Vallen Acoustic Emission data file... shows six isolated disturbances within the fiber during an overnight test run.

**Figure 7: Vallen Visual Acoustic Emission diagram showing six incidences of possible internal**



Using the wave applet feature of the Vallen Acoustic Emission system, a particular Vallen Visual AE diagram was analyzed and converted into a 3 dimensional image of the respective hit's frequency. These images consisting of 4 peculiar hits illustrates a possible micro crack detection. Upon reviewing these graphs, there exists a slight difference in the wavelet coefficient and the intensity of the 3D graphs in direct correlation to their respective energies. This correlation, in future tests, may establish a way for determining deformations

within the fused silica fiber. In addition to verifying these deformations, it may be possible to determine the crack width, geometry, and location. Although crack length and geometry may prove to be most challenging within the allotted programs, finding the source of propagation can be achieved by analyzing the recorded hit energy. If the energy appears to be greater near a particular accelerometer then the disturbance originated close to that particular piezoelectric. In this case, the energy appeared higher near the test mass. In similar response, the energy appeared diminished near the mounting bracket or "red" sensor.

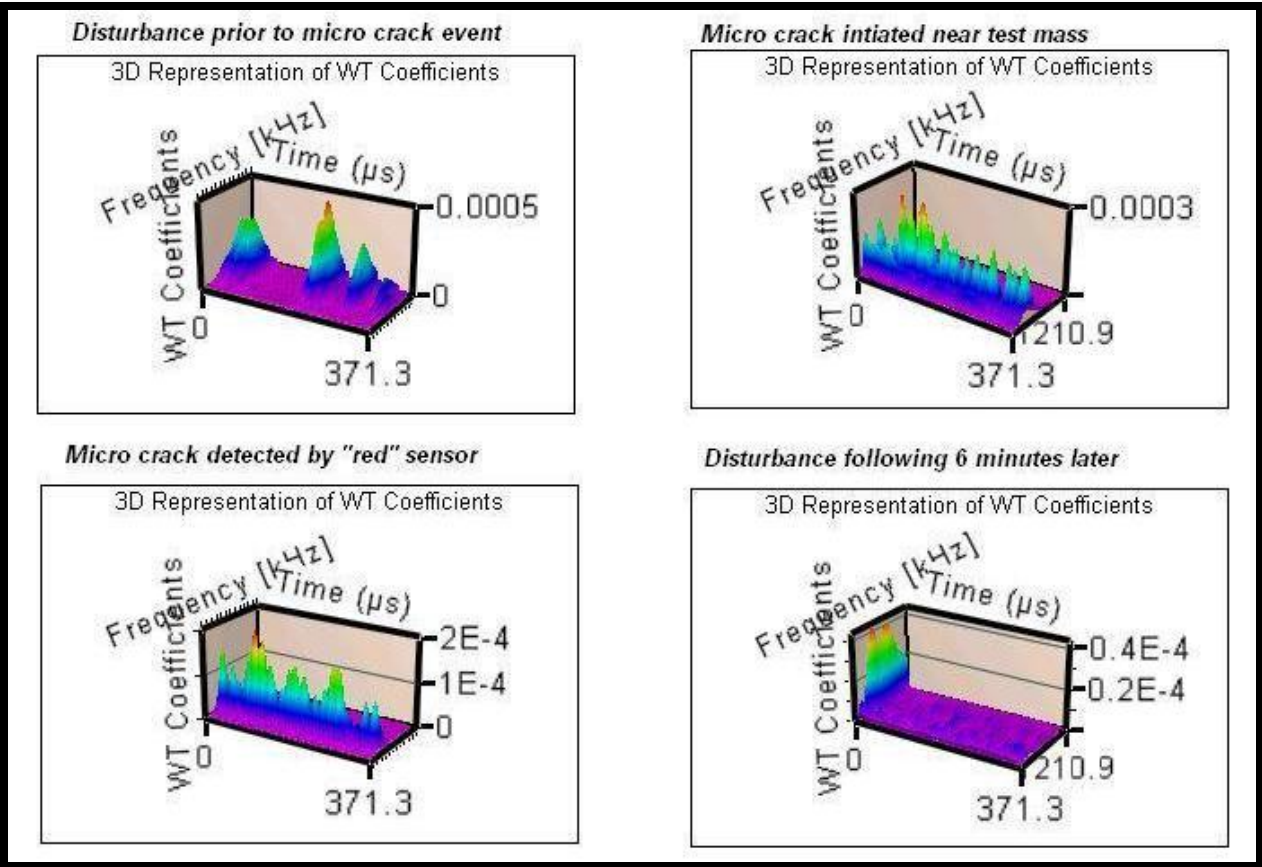
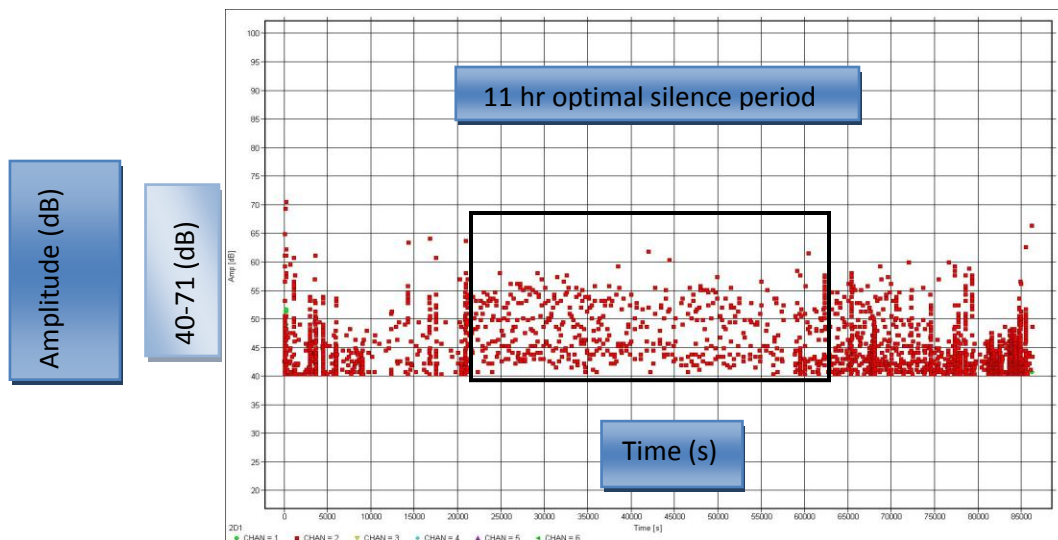


Figure 8: Possible micro crack detection as depicted by this 3 dimensional progression.

2.6 Electromagnetic interference (EMI)

When using piezoelectric accelerometers, several factors must be taken into consideration in order to eliminate as much background noise as possible. To name a few extracurricular inputs not pertaining to vibration related outputs, transverse vibrations, poor mounting, base bending, high sound levels, humidity,

high and low temperatures, x-rays, gamma rays, and electromagnetic fields all contribute to false vibration measurements. Eliminating several known erroneous inputs, the remaining false input that shall be discussed, as it is one of few verified false signatures, pertains to electromagnetic fields. This electromagnetic interference or "EMI" emanates from laboratory lighting as denoted by several Vallen Visual AE diagrams. Reviewing the data and comparing the densities of hit points, the amount of vibrations recorded within the system appear to be greater during the day. Shedding even more light on the situation, alternating the current by switching the above laboratory lights on and off produced sudden spikes in the Vallen Visual AE diagrams. If this alternation endured for a significant amount of time then consistent streams of background noise emerged. This inductive coupling originated from the proximity of cables carrying high AC currents. "Current spikes" coming from quickly switched circuits and other high frequency currents may also produce this source of electromagnetic interference. Fortunately, this emergence dissipates over a given period of time. However, this dissipation period constricted accurate data analysis to a minimal acquisition period. As a cleaning tool, the pulsing capability of this particular piezoelectric accelerometer enables one to actively reduce these false signatures. After proactively inducing an electromagnetic interference, initiating pulses from either channel will automatically counter this EMI. For future tests, magnetic shielding should be taken into consideration.



**Figure 9. A Vallen Visual AE diagram depicting a 20 hour acquisition run with an 11 hour optimal silence period as a result of an absence in light and human activity.**

## 2.7 Pulse Method

Vallen Visual AE data showed echoes in most diagrams while pulses were emitted from channel 1 and channel 2. If the acquisition recorded pulses for an extended period of time then several echoes emerged. These echoes or receiver counterparts proved to be quite useful for analyzing particular aspects of how the pulse effected the fiber. In reference to the existence of cracks in the material, these pulses led to further deformation investigations. Using these pulses established a method that could be controlled and monitored. With this Pulse Method, in order to identify external disturbances pulses were sent through both channels and studied. The echoes hit energy, time delay, and amplitudes were recorded. Pulsing also illustrates the direction of the wave propagation. In reference to the figure(indicate) below, if pulses are input from the test load then the difference in amplitude between the two sensors appears greater than pulses emitted from the sensor attached to the mounting bracket. (Record amplitude diff) Also, during this particular run (refer to graph) the reception of pulses at the top showed displayed hits of slightly different amplitudes and energies. The pulses received at the base followed a more linearly consistent pattern. (record amp and at what time duration)

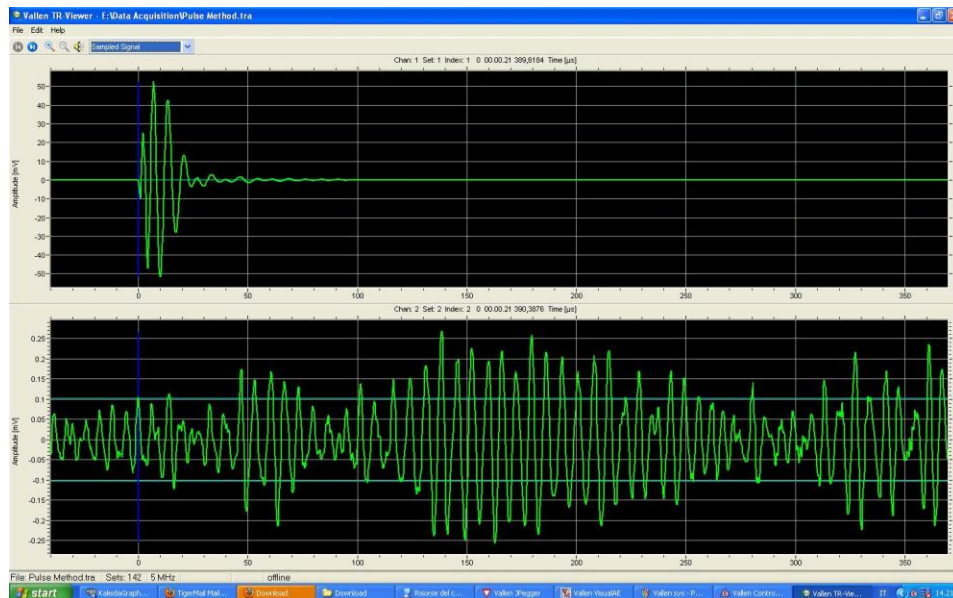
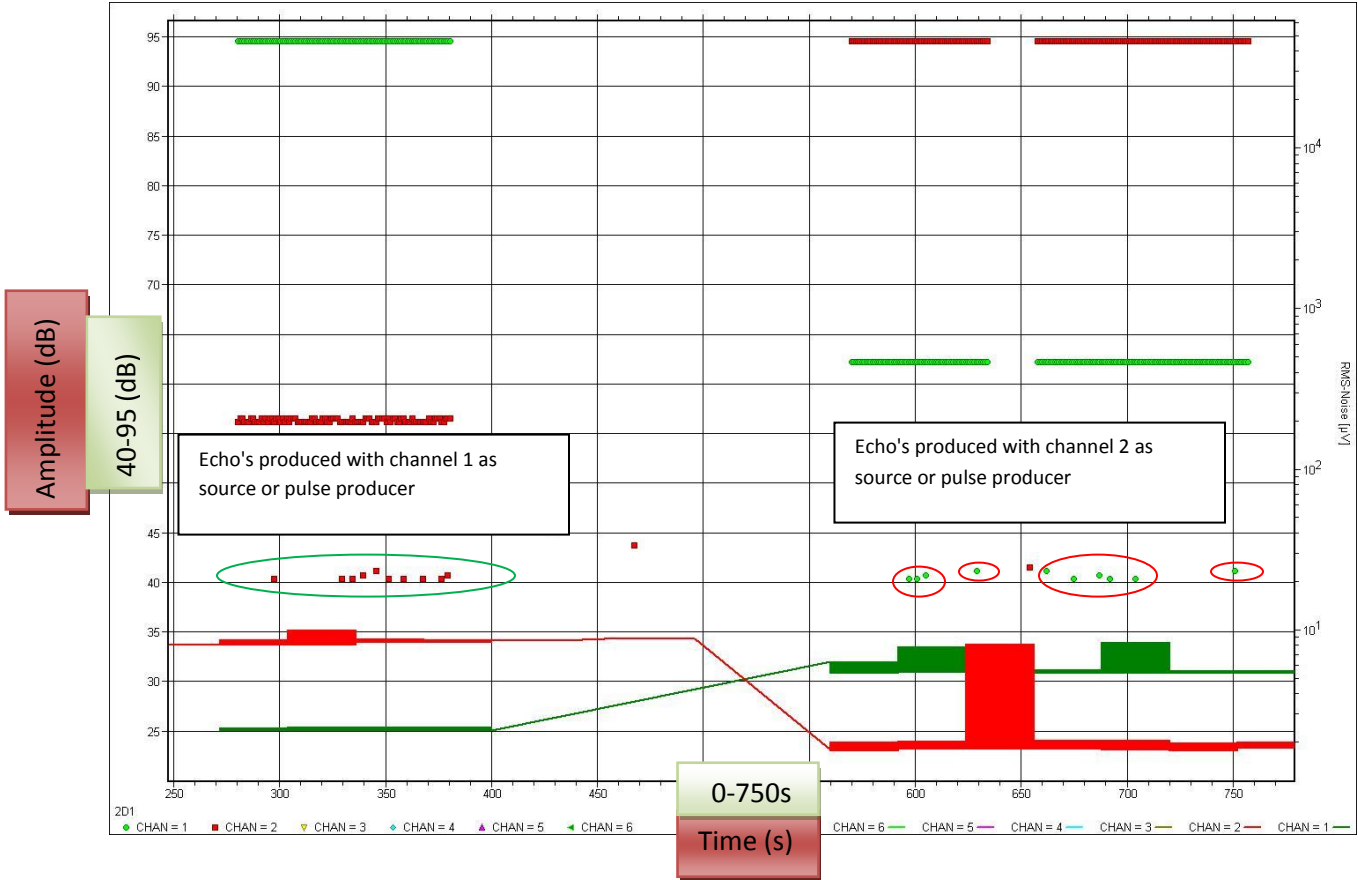


**Figure 10. Image of a Vallen Visual TR Viewer graph of a pulse sent through channel 2 (top) and recieved by channel 1 (bottom)**

Figure 11. Vallen Visual AE diagram showing "hit" depicting echoes from both channel 2 and channel 1 counterparts respectively



Id	DSET	CHAN	A	R	D	CNTS	E(TE)	RMS	THR	PAO	FLAG	HHHNS	MSEC	NSEC	
			[dB]	[μs]	[μs]		[eV]	[μV]	[dB]	[mV]	MRSFXCTAEDN	[hhmmss]	[ms.μs]	[ms.μs]	
Hit	573	2	56,5	280,0	10256,0	875	155E02	8,2	40,0	0,938	R	c	00.05.24	459,8134	459,813400
Hit	576	1	94,5	7,0	114,6	17	167E04	2,4	40,0	0,625	C		00.05.25	459,5364	459,536400
Hit	577	2	56,5	279,8	11369,6	869	162E02	8,1	40,0	0,625	R	c	00.05.25	460,2207	460,220700
Hit	580	1	94,5	7,0	114,6	17	167E04	2,4	40,0	0,625	C		00.05.26	459,9436	459,943600
Hit	581	2	56,5	280,2	11372,8	913	164E02	8,2	40,0	0,625	R	c	00.05.26	460,6276	460,627600
Hit	584	1	94,5	7,0	114,6	17	167E04	2,4	40,0	0,938	C		00.05.27	460,3508	460,350800
Hit	585	2	56,5	280,0	11286,4	904	160E02	8,1	40,0	0,938	R	c	00.05.27	461,0350	461,035000
Hit	588	1	94,5	6,8	114,6	17	167E04	2,4	40,0	0,313	C		00.05.28	460,7581	460,758100
Hit	589	2	56,2	279,8	11356,8	868	159E02	8,1	40,0	0,313	R	c	00.05.28	461,4424	461,442400
Hit	592	1	94,5	6,8	114,6	17	167E04	2,4	40,0	0,625	C		00.05.29	461,1653	461,165300
Hit	593	2	56,2	279,8	11372,8	896	162E02	8,4	40,0	0,625	R	c	00.05.29	461,8494	461,849400
Hit	595	2	40,4	0,2	0,2	1	221E-1	9,9	40,0	0,313			00.05.29	466,8716	466,871600
Hit	602	1	94,5	7,0	114,6	17	167E04	2,4	40,0	0,938	C		00.05.30	461,5724	461,572400
Hit	603	2	56,2	280,0	11414,4	877	163E02	8,4	40,0	0,938	R	c	00.05.30	462,2565	462,256500
Hit	606	1	94,5	6,8	114,6	17	167E04	2,4	40,0	0,313	C		00.05.31	461,9797	461,979700
Hit	607	2	56,2	280,0	11302,4	881	161E02	8,4	40,0	0,313	R	c	00.05.31	462,6638	462,663800
Hit	610	1	94,5	6,8	114,6	17	167E04	2,4	40,0	0,000	C		00.05.32	462,3869	462,386900
Hit	611	2	56,2	280,0	10252,8	833	156E02	8,4	40,0	0,000	R	c	00.05.32	463,0710	463,071000
Hit	614	1	94,5	7,0	114,6	17	167E04	2,4	40,0	0,625	C		00.05.33	462,7940	462,794000
Hit	615	2	56,2	280,0	11587,2	896	162E02	8,4	40,0	0,625	R	c	00.05.33	463,4782	463,478200
Hit	618	1	94,5	6,8	114,6	17	167E04	2,4	40,0	0,625	C		00.05.34	463,2013	463,201300
Hit	619	2	56,5	280,0	11372,8	891	163E02	8,4	40,0	0,625	R	c	00.05.34	463,8853	463,885300
Hit	621	2	40,4	0,2	0,2	1	329E-1	8,4	40,0	0,625			00.05.34	483,1449	483,144900
Hit	624	1	94,5	6,8	114,6	17	167E04	2,4	40,0	0,313	C		00.05.35	463,6085	463,608500

Figure 12. Vallen Visual AE display of a "hit" chart indicating the amplitude, count, energy, and time.

## 2.8 Silica Bonding

As a component of understanding the fiber's behavior, exploring the bonding capabilities is required as the fiber is too fragile for any type of welding. Gluing the fibers as a means of attaching the fiber to the interferometer mirror is the better option. Similar to the fused silica fiber, the bonding agent must be a clean solution, possess ultra high vacuum compatibility, and be non-dissipative. Adjoining the fiber and the mirror, an intercessor is used. This intermediary is more commonly known as the "ear" of the construct. As seen below in figure 11, the ear serves as a supporting block. Reconfiguring the Si-O bonds in  $\text{SiO}_2$  chains, the silicate bonding procedure is the alternate method for attaching or "gluing" silica fibers. This bonding procedure uses extremely pure components such as flat surfaces, ultra-pure water, and the catalyst potassium hydroxide (KOH). The procedure begins with hydration where a drop of a pure dilute KOH solution is used to wet the surface being glued. Next, etching occurs from the KOH solution because of the presence of the  $\text{OH}^-$  groups. As a result of this presence, Si-O bonds are broken and  $\text{SiO}_3^{2-}$  are produced in the solution. The last step involves dehydration.  $\text{OH}^-$  strips the  $\text{H}^+$  from the silanol group on the surface forming water. Si-OH groups dehydration produces Si-O-Si bridges. Ultimately, the  $\text{SiO}_3^{2-}$  chains connect the two surfaces completing the gluing procedure.

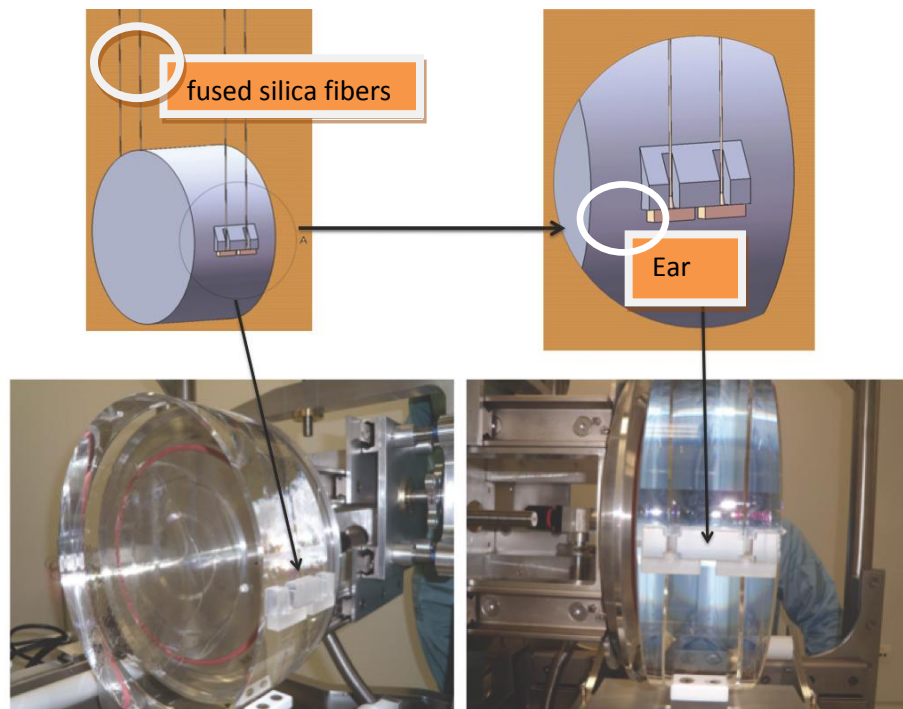


Figure 13. Images of interferometer mirror with fused silica fibers attached.

### 3 Experimental Results

#### 3.1 Speed of sound

Using the Vallen Visual AE diagram, time measurements were made during preliminary tests. Pulses were sent through the given fiber. As pulses were received from the non pulsating piezoelectric accelerometer, reception times were recorded. These differences in time were displayed on the Vallen Visual AE value chart. The measured Steel wire length was .7938 m. Using the equation for velocity and with this given length and a time delay of (number), the resultant velocity for the speed of wire within the Steel wire was (number).

$$v = \frac{\Delta x}{\Delta t}$$

The expected value as calculated by using the young's modulus and fused silica density.

$$v = \sqrt{\frac{\text{(Young's modulus equation)}}{\text{Density}}} = \sqrt{\frac{Y}{\rho}}$$

Likewise, this method of measurement was applied to the fused silica fiber. The fiber length, average time delay, resultant velocity were the following: .8m, .00029s, 2758 m/s.

Id	DSET	CHAN	A	R	D	CNTS	E(TE)	RMS	THR	PA0	FLAG	HHMMSS	MSEC	NSEC
			[dB]	[μs]	[μs]	[eu]	[μV]	[dB]	[mV]	MRSFXCTAEDN	[hhmmss]	[ms.μs]	[ms.μs]	
La Label 1: '12.58 Resume'														
DT giovedì 9 giugno 2011. Host Time: 12.58														
La Label 2: '12.59 Pulsing channel: 1'														
Ht	71	1	67.4	9.8	34.4	5	345E01	2.8	40.0	0.000	C	00.00.51	376.0556	376.055600
Ht	72	2	49.0	78.8	1088.0	70	752E00	8.9	40.0	0.000	c	00.00.51	376.3215	376.321500
Ht	75	1	67.4	9.8	34.4	5	346E01	2.7	40.0	0.313	C	00.00.52	376.4628	376.462800
Ht	77	2	49.0	55.6	1078.4	72	754E00	8.9	40.0	0.313	R c	00.00.52	376.7518	376.751800
Ht	80	1	67.4	9.8	34.4	5	345E01	2.8	40.0	0.000	C	00.00.53	376.8700	376.870000
Ht	81	2	49.0	75.8	1109.2	71	770E00	8.9	40.0	0.000	c	00.00.53	377.1390	377.139000

Figure 14. Vallen Visual Acoustic Emission (AE) hit information display chart. As indicated above, these hits are a result of pulsating the accelerometer by pulsing channel 1.

### 3.2 Fast Fourier Transform

Two fast Fourier transform (FFT) plots were produced using the Vallen acoustic emissions program FFT avg applet. The first plot (figure 13) represents pulses emitted from channel 2 and the output as denoted by channel 1 is seen through the second plot (figure 13). Another set of plots were taken in the same fashion, however; the pulses were sent through channel 1 and received by channel 2. A ratio of these two scenarios were taken and are being analyzed by researchers at the University of Rome.

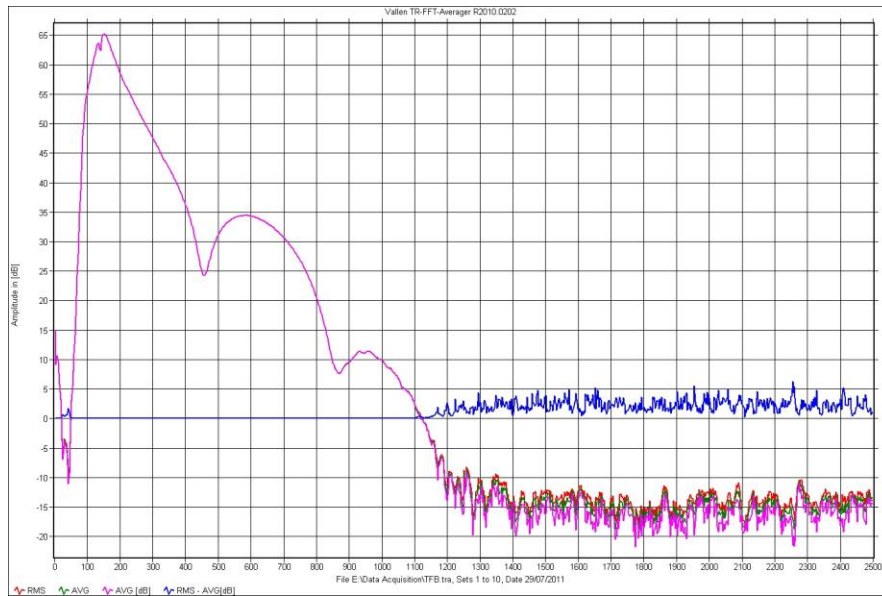


**Figure 15. Image of FFT depicting waveform produced by pulses sent through channel 2**

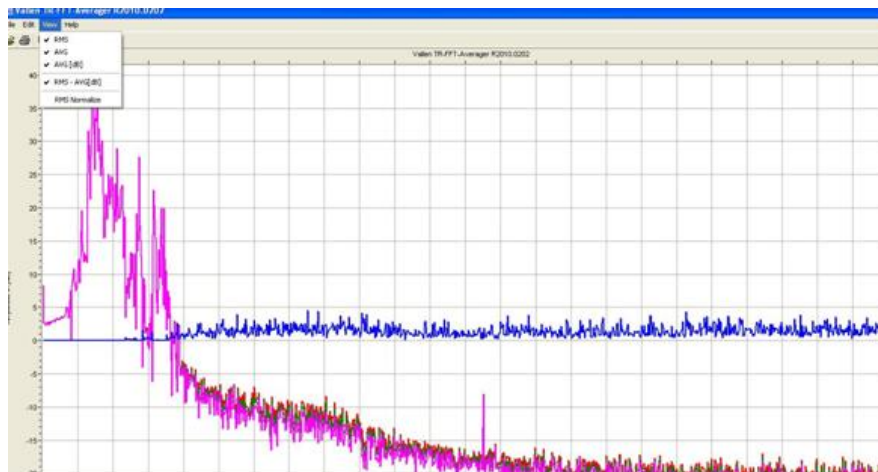


**Figure 16. Image of FFT depicting waveform produced by pulses received through channel 1**

## **4 Conclusion**

The acoustic emission analysis of silica fibers described in this report has several applications for understanding the properties of the fused silica fiber. With further investigations, deformations as well as events that occur prior to a possible break in the fiber can be isolated and studied. After shielding the piezoelectric from electromagnetic disturbances, properly securing the cables attached to these accelerometers, and establish an even, smooth wax distribution on the contact surface; proper silent runs can be achieved. With an insulated system, fibers can be analyzed thoroughly and efficiently. Also, in order to reduce mechanical noise, an apparatus that allows for a dually decoupled system may reduce virtually all sources of external noise. This dually decoupled set up would detach both piezoelectric accelerometers from the mounting frame. Therefore, with a decoupled system future fused silica fibers can be analyzed in complete silence.

## **Acknowledgements**

I would like to thank the National Science Foundation for funding this summer IREU program, the University of Florida Physics Department for offering me this incredible opportunity, and the University of Rome, "Sapienza" in Rome, Italy. Also, I would like to thank Paola Puppo, Andrea Conte, Maurizio Perciballi, Ettore Majorana for helping me throughout the course of this summer. Finally, I would like to send a special thank you to Andrew Dwayne Spooner for scientific inspiration.

## 5 References

Bruel & Kjaer, *Piezoelectric Accelerometers and Vibration Preamplifiers*

The Vallen system AMSY-5 User Manual

P. Amico, L. Bosi, L. Carbone, L. Gammaitoni, F. Marchesoni, Michele Punturo, F. Travasso, H. Vocca, *Monolithic fused silica suspension for Virgo gravitational waves detector* Vol 73, No. 9 September 2002

Leak Detector Methods: A comparative Study of Technologies and Techniques Short Version

Michele Punturo, *Monolithic Suspension*

S. Rowan, J. Hough & C.A. Cantley, *Bonding & visual inspection of preliminary test ears*, July 2005